Method development for the synthesis of large crystals of pyromorphite

Laura W. Y. Lo
Email: Laura-lo@hotmail.co.uk or U1267189@unimail.hud.ac.uk

Abstract
In the UK, water utilities add phosphate to drinking water in order to prevent lead being released from older properties that are supplied by lead water pipes. The mechanism of reduction is thought to involve the formation of insoluble lead phosphates. This research was carried out to optimise the growth of large lead apatite crystals for use in future atomic force microscopy work. In this case study, pyromorphite crystals exhibiting both prismatic hexagonal and needle-like structures with sizes up to 0.2mm were successfully grown using a caesium chloride flux. They were produced both at lower temperatures and in less time than previous studies. All samples were characterised using a variety of analytical techniques such as X-ray diffraction, infrared spectrometry, energy dispersive X-ray analysis, scanning electron microscopy and thermogravimetric analysis.

Keywords: Pyromorphite; apatite; lead; crystal growth; phosphates; water treatment.

Introduction

To date, research has been limited on the production of large lead phosphate crystals of pyromorphite. Naturally, large-sized lead phosphate crystals are hard to come by, therefore the research goal of this study was to produce a methodology that gives reproducible results for the formation of crystal particles of a larger size (mm+) than were initially synthesised (approximately 250nm). With the use of an atomic force microscope, the production of larger-sized crystals will then enable the advancement of future work in trying to understand their functionality in how they grow and dissolve within lead water pipes.

The study aims to incorporate certain aspects as well as improve on previous concepts used within crystal synthesis, to research whether the production of larger-sized crystals with high crystallinity is possible in a controlled environment. It is hoped that this will result in the optimisation of traditional methods, as well as obtaining crystals of larger size.

Lead metal
Pure lead, the 82nd element found in the periodic table, contains a bright lustre with a silvery metallic appearance. When exposed to moisture, the lead tarnishes and darkens due to the oxide coating formed on the surface that seals the underlying element, and thus halting it from further corrosion.[1] The metal itself crystallises in a face-centred cubic structure,[2] and is commonly found in small concentrations in the Earth's crust. Although rarely found in its pure state, the metal appears in the form of lead ores, galena (PbS) and anglesite ($PbSO_4$).[3]

Today, lead is a known neurotoxin, with studies recently highlighting the lasting behavioural effects on children, even with low blood levels of 10μg/dL.[4] The amount of exposure to the population is of importance to environmental chemists, who try to limit the amount of lead within the atmosphere. The last 30 years has seen the amount of lead levels in the environment drop considerably, coinciding with the termination of the use of tetraethyllead (TEL) in petrol, which was once used as an octane-boosting compound,[5] as well as lead elements that were once popularly used as pigments in paints.[6]

Unfortunately, lead can be considered a 'close to home' contaminant, making it difficult to regulate and monitor precisely. It has been found that one of the major routes of entry into the body is by ingestion through drinking tap water, contributing to 10–20% of a child's total lead intake.[7] This varies between different areas of the UK, and is highly dependent on whether lead water pipes that were used in houses built before the 1970s have been replaced in recent years. These pipes are generally found beneath the garden and connect the house to the mains water pipe from the street, although in some cases, parts of a pipe made from lead can be found inside the home; both these circumstances result in lead-contaminated water being supplied to the main house taps.[8]

Phosphate dosing
Tap water characteristically begins with virtually no lead contaminants when freshly sourced. The problem begins when water passes through old, corroded lead pipes, which enables lead to dissolve into the water. This acknowledgement, as well as the constantly decreasing legal limit of lead concentrations in tap water, which in the UK is currently aiming for the European Union lead limit of 10μg/L,[9] has encouraged water suppliers to begin treating tap water with orthophosphate dosing.[10] This is a cheaper alternative than widespread lead pipe removal and replacement.

Phosphate ions (PO_4^{3-}) exist in three forms, orthophosphates, metaphosphates (also known as polyphosphates), and the ester form of organophosphates. All three contain phosphorous, but in different chemical rearrangements.[11] In general, most phosphates

are insoluble or only slightly soluble in water. The phosphates used in water treatments can be dosed as phosphoric acid, polyphosphates, or mixtures of zinc orthophosphate with orthophosphoric acid, and orthophosphoric acid plus polyphosphate.[12]

Colling et al. originally discovered phosphate dosing in the 1980s, and this effectively induced the industry to implement the addition of phosphates to tap water, contributing to the considerable reduction of lead.[13] Phosphate dosing works by inhibiting the ability of lead to dissolve in water by encouraging the formation of a low-solubility phosphate deposit, pyromorphite ($Pb_5(PO_4)_3Cl$). This compound works by forming a thin layer on the inner surface of a pipe, preventing lead leaching.[14] In recent studies, it has also been found to possess the ability to trap other harmful elements, such as arsenic.[15]

Apatites
Out of all the phosphate minerals, the apatite group is by far the most prolific,[16] existing in more than 150 forms in the lithosphere.[17] The accessibility of phosphorous depends heavily on the degeneration rate of phosphate-containing minerals, such as the apatite group.[18] The rate can be increased by acidifying a region consisting of high concentrations of these minerals. This can also be used to explain why acids erode tooth enamel, a highly mineralised substance made up of layers of hydroxylapatite, a member of this apatite group.[19]

The structure of apatite is considered to be extremely tolerant of ionic substitutions, resulting in the common occurrence of paired substitutions in apatites. In terms of water treatment, manufactured hydroxylapatite ($Ca_5(PO_4)_3OH$) have been widely used to remove lead (Pb) from aqueous mixtures. They act as containment agents by cation exchange, due to their ability to remove heavy metal ions with valency two from contaminated water. This works by first allowing the toxic lead to adsorb onto the surface of the hydroxylapatite, allowing the exchange to take place. This results in the formation of the lead apatite known as hydroxylpyromorphite ($Pb_5(PO_4)OH$), in which all the available cation sites are occupied by lead (Pb) (II) ions.[20] These lead forms of pyromorphite are one of the least soluble among the apatite group, even over a wide range of pH; this is coupled with a very high thermal stability.[21] This basis give these minerals, whether they were naturally or synthetically formed, the ability to immobilise harmful and radioactive metal ions.[22]

Crystal structure
The crystal structures of apatites are identifiable by their prismatic hexagonal symmetry, with space group P6/m.[23] What is generally found in lead apatites is that the separated orthophosphate group (PO_4^{3-}) tends to be based in a tetrahedral position to Pb^{+2}, producing a neutral solid when a singly charged species such as a chloride ion (Cl^-) is linked along the *c* axis, producing pyromorphite.

However, in previous studies, two forms of structures, hexagonal and monoclinic, have been recorded in which the structural outcome depends on the stoichiometry, pressure, and temperature of the experiment conducted.[24] In relation to the lead apatites, the hexagonal arrangement is usually associated with nonstoichiometric compounds, whereas the stoichiometric version takes on the monoclinic form. This is directly correlated to the problematic nature of producing stoichiometric apatites due to their tremendous agility in accommodating substitutions.[25] In relation to this, the lattice energy can also be affected within the pyromorphite structure. It was identified that out of all the substituted pyromorphite minerals, the unaltered pyromorphite form with chloride contained the smallest lattice energy, confirming it to be the most stable structure. This stability was reported to change as the amount of substitutions of lead increases, by the accommodation of cadmium and zinc (II) ions.[26]

In relation to the structure, it has been stated in previous studies of apatites that at room temperature, the mineral obeys a monoclinic structure with four formula units per

cell. Phase transitions into a hexagonal arrangement with two formula unit cells occurs at around 310°C to 370°C for the pyromorphite group.[25]

Crystal growth
A small number of research methods have previously been proposed to give good single crystals of pyromorphite. A common technical approach that has been used in past research to successfully synthesise general crystals is the inclusion of a standard flux technique.

The technique is largely used when crystals exhibit the need to be freed from thermal tension. The required complex is usually dissolved in a solvent that acts as the flux. The reaction proceeds in an atmosphere-controlled furnace at temperatures above the melting points of both substances, to enable complete saturation. Because of this, the experiment commonly takes place in a lidded crucible made from highly stable, temperature-resistant materials. Typical materials could be platinum and niobium, which are frequently used in the growth of oxide crystals, as these possess melting points of 1768.2°C[27] and 2469°C,[28] respectively. On the other hand, the crucible material used for the formation of metallic minerals with large crystal structure can range from alumina and zirconia, which both have melting points of over 2000°C.

Once the sample has been held for an appropriate amount of time, the crucible is normally permitted to cool at specific rates (usually very slowly) to enable the formation of a newly self-organised thermodynamic phase, to precipitate out of the cooling aqueous mixture. Though it is a common approach in crystal growth, it is rare to form crystals with a size greater than a few centimetres.

A method originally produced by Aoki et al.[29] documented the ability to produce 1mm crystals using excess lead chloride acting as the flux. However, the reproducibility of these results using this method has been questioned due to the number of repeated failed attempts by other researchers in this field.[30]

As a result of this, Masaoka et al.[30] further developed this flux technique to introduce what is called a caesium chloride flux, with the caesium chloride acting as the solvent. The technique involved starting off with a mixture of finely ground powders of pyromorphite and mimetite ($Pb_5(AsO_4)Cl$). The mixture was placed with different ratios of the caesium chloride flux, packed into a 30ml platinum crucible and sealed with a platinum lid. The mixture of all three compounds was then placed into a furnace and heated to 900°C with a nitrogen flow. From the research, it is apparent that 1mm hexagonal prismatic crystals were successfully formed at around 500°C and followed with a cooling rate of 5°C h^{-1}.

Other relevant methods include using crystallisation heat treatment, which is a recent technique followed by Denry et al.[31] to produce fluoroapatite glass-ceramics. The research saw specimens heat-treated to reach high temperatures of up to 1525°C, coupled with using variable rates of heating and cooling to promote a change in the crystal morphology.

In order to produce high-crystallinity apatite, the most common approach is to use high-temperature processing, a usual methodology for the production of numerous calcium phosphates. These compounds are of similar formula and structure to the lead apatites discussed in this present research. In recent papers by Tõnsuaadu et al.,[32] it is noted that heating to temperatures of 600–1000°C enhances the lattice structure, removing the majority of additives from the synthesis stage to yield a more pure form of the desired apatite. It was also found that further heating to around 1360°C produced very stable calcium phosphate compounds with high crystallinity, a similar structure to the desired lead apatite needed in this research. This study confirmed the ability of apatites to form a larger crystal structure through high-temperature processing, as well as affirming the stability of apatites at very high temperatures.

Project plan

As outlined above when exploring crystal growth, it is necessary to use temperatures significantly higher than the melting points in order to form larger crystals with the desired structure. But in order to reach this stage, the original powder form of pyromorphite needed to be synthesised and followed by characterisation using both X-ray diffraction (XRD) and infrared spectroscopy (FT-IR).

Due to the lack of research in the area of pyromorphites, there were no known literature values for the exact melting point or the behavioural effects of the phosphate at certain temperatures. Therefore, the stability of pyromorphite was analysed using an analytical technique called differential scanning calorimetry (DSC). This was followed by the use of thermogravimetic analysis (TGA) to heat small samples of the lead phosphates to determine whether crystals would form from a melt. The TGA allowed small trial experiments to be run on the samples at different temperatures to determine which temperature gave the best crystallinity of pyromorphite. This was analysed using XRD.

This data gave a foundation of experimental parameters, which began a series of scale-up experiments that took place in a nitrogen tube furnace. Larger samples were used while alternating the heating and cooling rates to different temperatures, to establish which parameter worked best in the formation of larger pyromorphite crystals using a flux technique. The final crystal structure and size was confirmed using a variety of characterisation techniques such as XRD, energy dispersive X-ray analysis (EDXA), and scanning electron microscopy (SEM).

Materials
The raw materials used within the synthesis of pyromorphite were all acquired from Fisher Scientific with the exception of sodium chloride, which was obtained from Sigma Aldrich. The water purifier used to produce the ultra-pure water with a resistivity of $18M\Omega$ cm was a Barnstead Nanopure from Thermo Scientific. An Eppendorf 5702 centrifuge was used to isolate the samples before they were dried in a silica gel based desiccator.

Methodology

Synthesis of pyromorphite
The chemical equation for the production of pyromorphite can be written as:

$$5Pb(NO_3)_2 + 3H_2NaPO_4 + NaCl \rightarrow Pb_5(PO_4)_3Cl + 7HNO_3 + 3NaNO_3$$
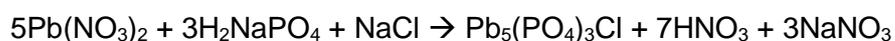
Starting with lead nitrate (0.04M), 25ml was pipetted into a clean 100ml volumetric flask. Into a second 100ml volumetric flask, 10ml of sodium phosphate solution (0.1M) and 15ml of sodium chloride solution (0.08335M) were pipetted. Both volumetric flasks were made up to the 100ml mark with ultra-pure water, then sealed and shaken thoroughly. The two solutions were then placed into two separate 250ml conical flasks. Gas dispersion rods connected to a nitrogen line by rubber tubing were then placed into each conical flask, and nitrogen was slowly bubbled into the solutions for approximately 20 minutes. After 20 minutes the conical flask containing the sodium chloride and phosphate mixture was placed onto a magnetic plate with a stirrer.

The pH of the sodium chloride/phosphate mixture was adjusted to 6 using carbonate-free sodium hydroxide (0.01M) and the slow bubbling of nitrogen gas continued. The lead nitrate solution was transferred to a clean dropping funnel and clamped above the chloride/phosphate solution. The funnel was then opened slowly, allowing the solution to fall in droplets into the conical flask over the course of around 20 minutes. Small additions of sodium hydroxide were needed to maintain the solution at pH 6 throughout.

Once both solutions were completely mixed, the nitrogen was left to bubble for a further 10 minutes. The overall solution formed a white cloudy precipitate, which was then poured into 80ml centrifuge tubes and centrifuged at 3500rpm for 3 minutes. This separated the precipitate from the water, which was poured away and was substituted with the remaining cloudy solution. This process was repeated until the entire product gathered in the bottom of the 80ml vessels. To ensure a clean and pure product, the vessels containing the product were then filled with ultra-pure water and centrifuged, and this was repeated five times. The water was removed from the sample, and the tubes containing the product were placed into a desiccator for 5 days. The dry product was then ready for analysis by XRD and FT-IR.

X-ray diffraction spectroscopy
Using a Bruker D2 Phaser, a small dried sample of the product was placed into an agate pestle and mortar, coupled with a few drops of methanol. This was then gently ground until a very fine white opaque liquid was present. Using a Pasteur pipette, the aqueous sample was transferred onto the centre of a Bruker AXS silicon sample holder. The methanol was allowed to evaporate off the surface, and the sample holder was then placed in position in the XRD. The measurement was taken using a scan between 5° and 100° 2θ, with X-ray radiation created by a copper Kα source.

FT-IR spectroscopy
A Thermo Nicolet 380 FT-IR equipped with a diamond crystal was used to gain the infrared spectra of the dried samples. The analysis was done between wavenumbers 4000 and 450cm^{-1}, followed by advanced attenuated total reflectance (ATR) correction and baseline adjustment to the spectra. The spectra were reduced to the region between 1500 and 450cm^{-1}.

Differential scanning calorimetry
Using a DSC1 Mettler Toledo, a DSC aluminium sample pan was filled with approximately 10mg of product. The lid was sealed using a universal crimper press and placed into position. The nitrogen flow was switched on at a rate of 80ml m^{-1} followed by the chiller with a constant temperature of 18°C. The samples were heated from 25°C to 600°C at a rate of 10°C min^{-1}. Once this was reached, the samples were left to isotherm for 5 minutes and cooled back down to 25°C at the same rate.

Thermogravimetric analysis
A TGA1 Mettler Toledo was used. For all runs, approximately 10mg of sample was placed in a TGA alumina crucible and sealed with an alumina lid. The sample was then placed into position, and a nitrogen gas flow rate of 50ml m^{-1} was set. The analysis consisted of heating from 25°C to 500/600°C and from 25°C to 1000°C, both at a rate of 10°C min^{-1}.

Nitrogen tube furnace
For all experiments, 0.2g of sample was mixed with 1.2g of caesium chloride flux and placed into a 4ml alumina crucible, sealed with an alumina lid. The parameters for the first experiment consisted of heating the mixture from 25°C to 700°C, with a heating rate of 300°C h^{-1}. Once this was reached, the temperature was held at an isotherm for 1 hour, before cooling back down to 25°C at the same rate. The second experiment used the same method, but the isotherm was increased to 5 hours. The third experiment followed the second method, with the temperature increased to 900°C. The fourth involved a new step that saw the incorporation of a very slow cooling stage. The sample mixture was prepared in the same manner as methods 1, 2 and 3, and then heated to 700°C at a rate of 300°C h^{-1} (5°C min^{-1}). The temperature was held at an isotherm for 5 hours then set to cool from 700°C to 600°C at a rate of 2°C h^{-1}. When the temperature reached 600°C, the furnace was set to cool back to 25°C at the rate of 300°C h^{-1}. All methods conducted were under a nitrogen atmosphere.

Crystal washing
Using a Pasteur pipette, approximately 1–2ml of ultra-pure water was pipetted into the crucibles containing the product. Using a micro spatula, the crystals were gently lanced from the sides of the crucible and mixed with the ultra-pure water to dissolve the caesium chloride flux. A Pasteur pipette was used to pipette the bottom of the crucible, gaining a more concentrated sample of crystals, and the solution was dropped onto the centre of a clean microscope slide. A cover slide was placed on top of the crystals, and any excess water was wiped away from the sides. The slides were then slowly placed into 1L beakers filled with an excess of ultra-pure water to allow any traces of the CsCl flux to dissolve in the water (approx. 500ml). The samples were left in the water for approximately 2–3 days, and then dried in a silica gel based desiccator. Once fully dry, the samples were ready for analysis.

SEM sample preparation
A small square of carbon-conductive double-sided tape was placed onto a metal SEM sample stub. The slide containing the sample was lightly pressed onto the adhesive tape, leaving a good coverage of crystals. The metal stub was then placed into the SEM sample holder ready for analysis.

Results and discussion

XRD spectra – synthesis

From inspection of the XRD spectra (Figure 1), it can be identified that the synthesis at room temperature produced the pure form of the desired product pyromorphite (PM). This is confirmed by the characteristic peak at the position 30° 2θ, in which a doublet appears. The spectra shows sharp peaks that indicate high crystallinity, verifying that the small crystals of pyromorphite have been successfully formed by this method. In comparison to the spectra published by Hopwood et al.[33] and the reference spectra found in the JCPDS database, the relative heights in the experimental spectra show good resemblance to the reference material, suggesting that no preferential orientation has taken place in the sample. There are also minimal shifts in the peaks when compared to the reference data, proving little or no difference in the crystal plain structure, and establishing that small pyromorphite crystals can be produced in this way.

Figure 1: XRD spectrum for pyromorphite powder
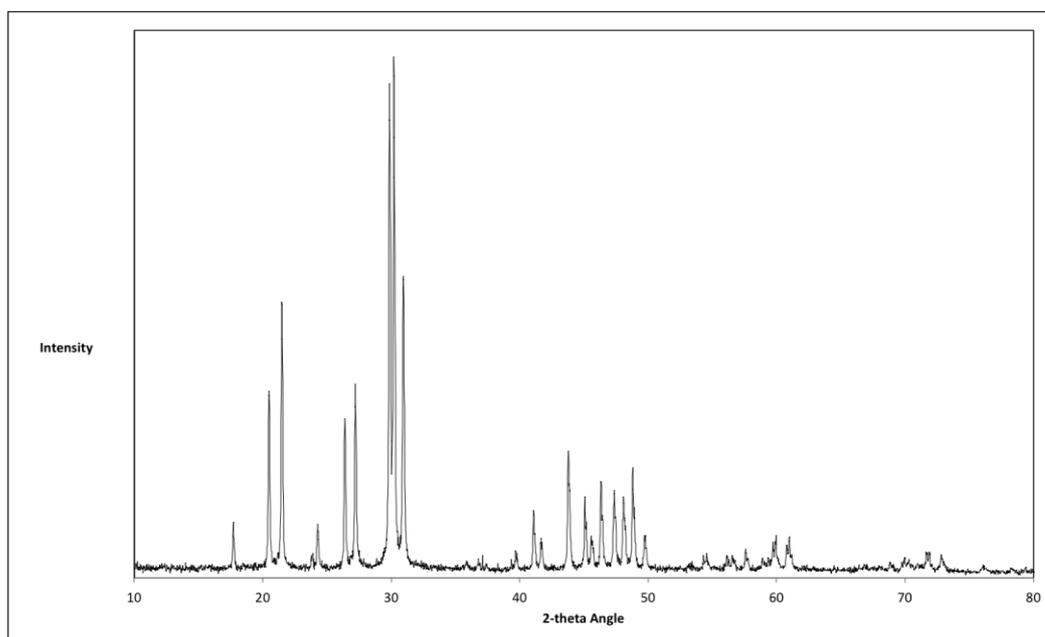
Crystal growth from a melt

A DSC curve for the heating and cooling of a pyromorphite crystal sample is shown in Figure 2. It can be seen that from around 130°C, there is a shallow exothermic drift in the baseline that continues all the way through the heating programme to 600°C. During this exothermic drift (exothermic up, in this case), there is a broad endothermic dip indicative of a phase transition. The type of transition can be either an endothermic decomposition reaction, whereby the product gases released take thermal energy away from the system, or the result of a change of state, such as a solid-to-solid rearrangement or a solid-to-liquid transition. This endothermic event starts in the region of 420°C and ends around 490°C, with a peak minima observed in the region of 465°C. At 600°C there is a sharp exothermic shift in the baseline due to a change in the method parameter. This is caused by an imbalance between the heat capacities of the sample and reference, which can also be the reason for the exothermic drift observed during the heating cycle. On cooling from 600°C to 120°C, there appeared to be no exothermic transition to indicate the reversal of the melting seen in the heating cycle. This suggests that the endothermic transition observed is more likely to be due to a small level of decomposition of the pyromorphite sample.

Figure 2: DSC curve for pyromorphite
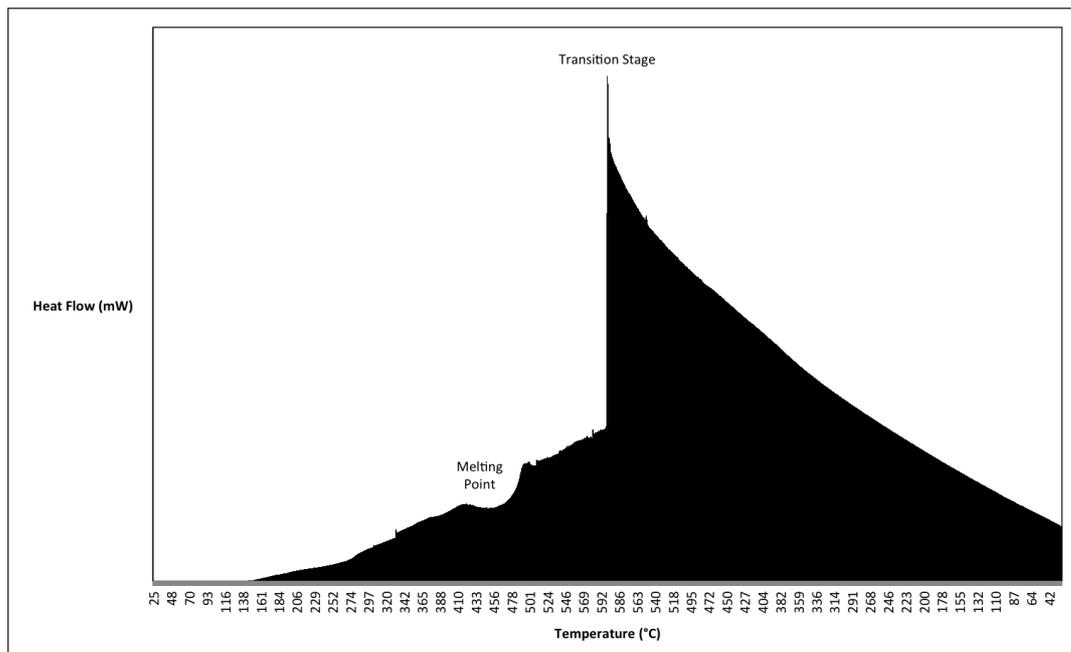
The main use of the TGA was to heat small samples to different temperatures to determine whether crystals would form from a melt and, thus, which temperature gave the best crystals of pyromorphite. Samples of pyromorphite were heated over a range of temperatures, reaching the maximum of the machine at 1000°C. The XRD spectra patterns were then taken for each temperature reached, and compared to each other. The spectra are shown in Figure 3.

Figure 3: XRD Spectra for TGA samples of pyromorphite
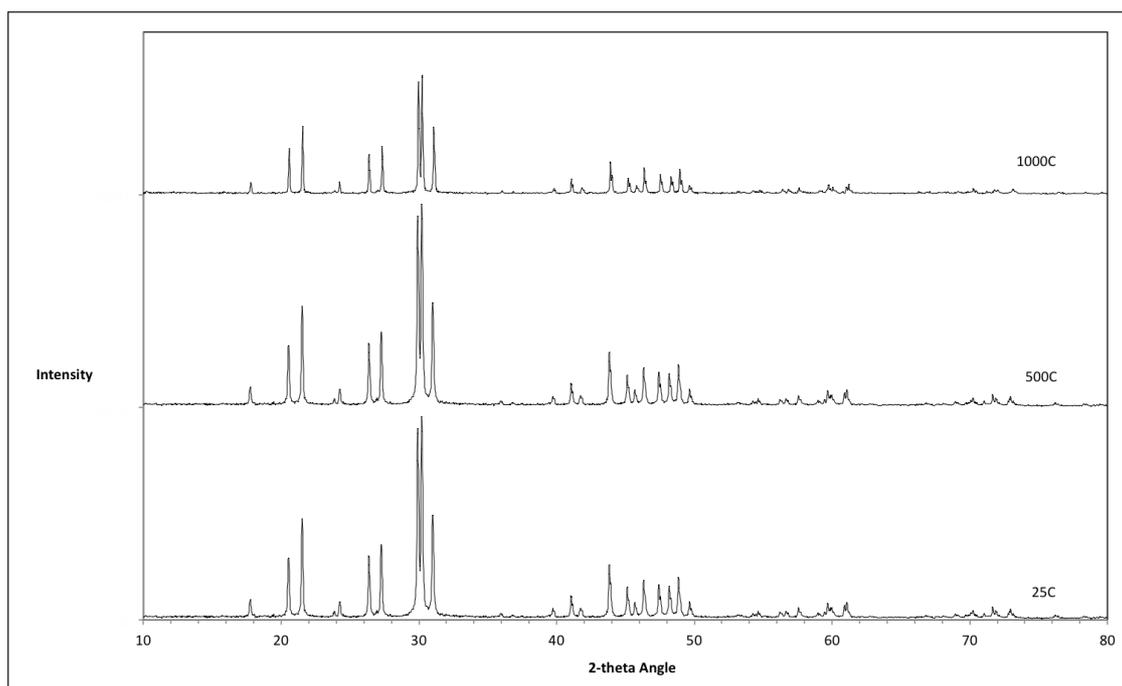
The XRD peak patterns for pyromorphite at each temperature look very similar to each other. This proves the pyromorphite structure is consistent throughout the thermal analysis (as confirmed by the DSC), but a slight sharpening of the peaks is observed for the pattern at 1000°C. This suggests that the sample formed a higher degree of crystallinity, indicating a long-range order of atoms compared to the lower temperatures. In addition to this, the physical state of pyromorphite remained stable throughout, but took on the appearance of a dark grey powder when cooled from 1000°C, suggesting that it was slightly over-heated during the analysis.

Crystal growth from a flux
From the DSC and TGA results, a set of parameters could now be established to begin the numerous experiments in the nitrogen tube furnace. The final results for all experiments performed are given in Figures 4–10. These display the different XRD patterns and SEM images, as well as the EDXA data for the crystals formed by the various experimental runs in which temperature, time and rate were changed subsequently.

XRD spectras

Figure 4: XRD pattern for pyromorphite and CsCl flux at 700°C from nitrogen tube furnace
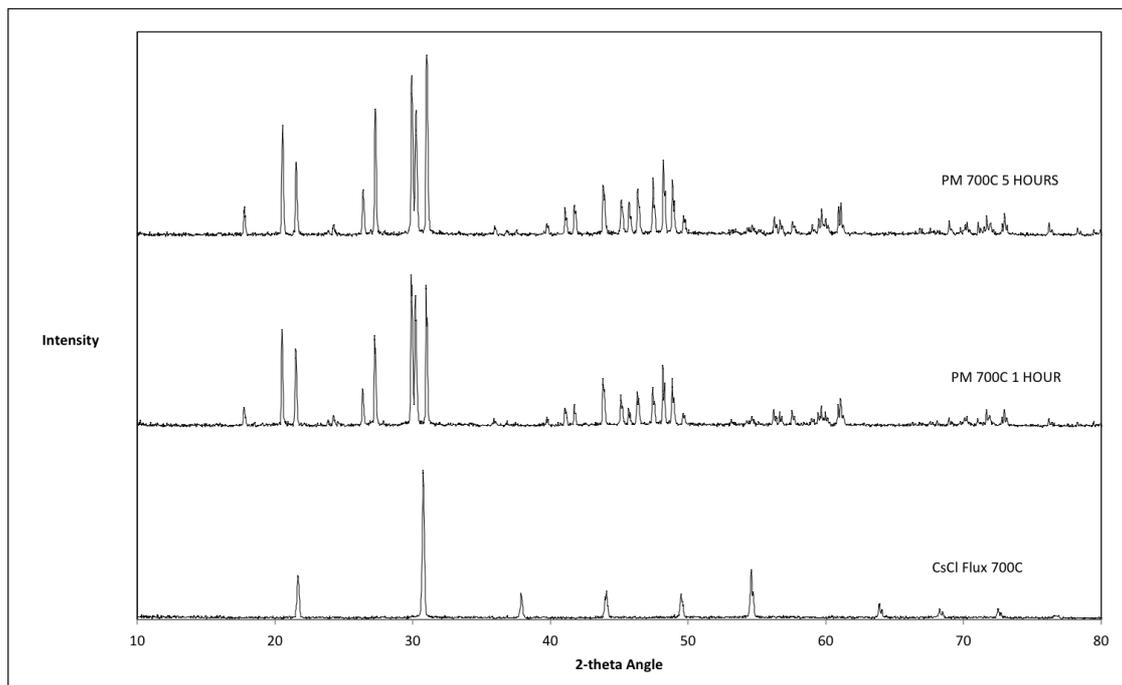
Figure 5: XRD pattern for pyromorphite and CsCl flux at 900°C from nitrogen tube furnace
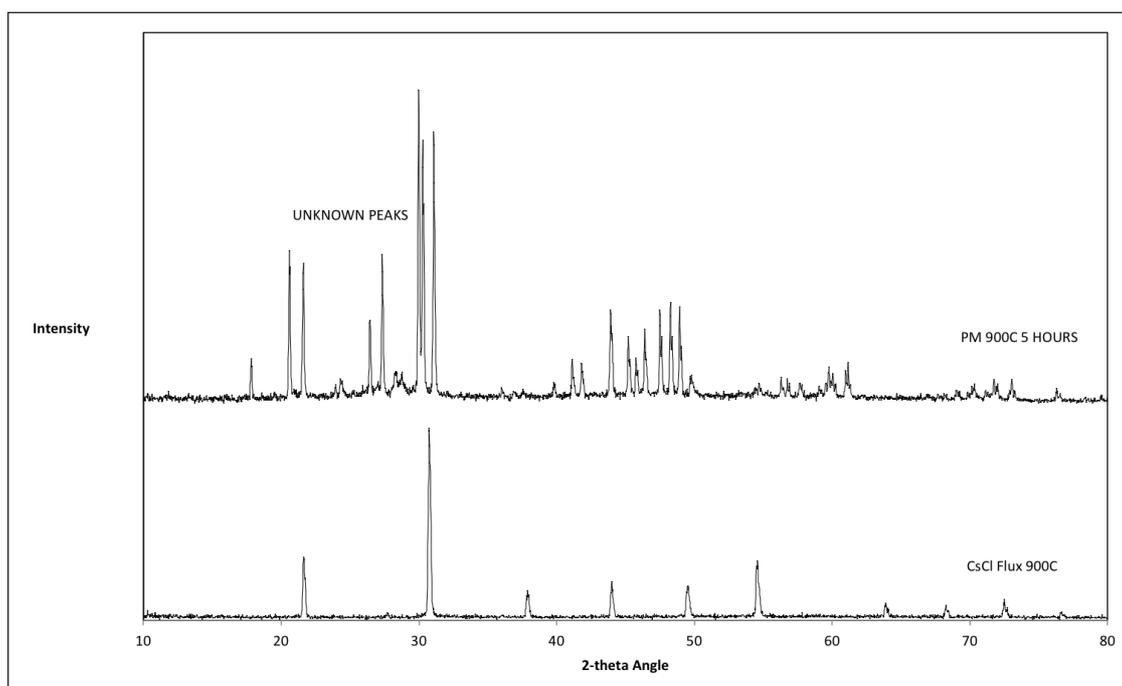
Figure 6: XRD pattern for pyromorphite and CsCl flux at 700°C with the addition of slow cooling from nitrogen tube furnace
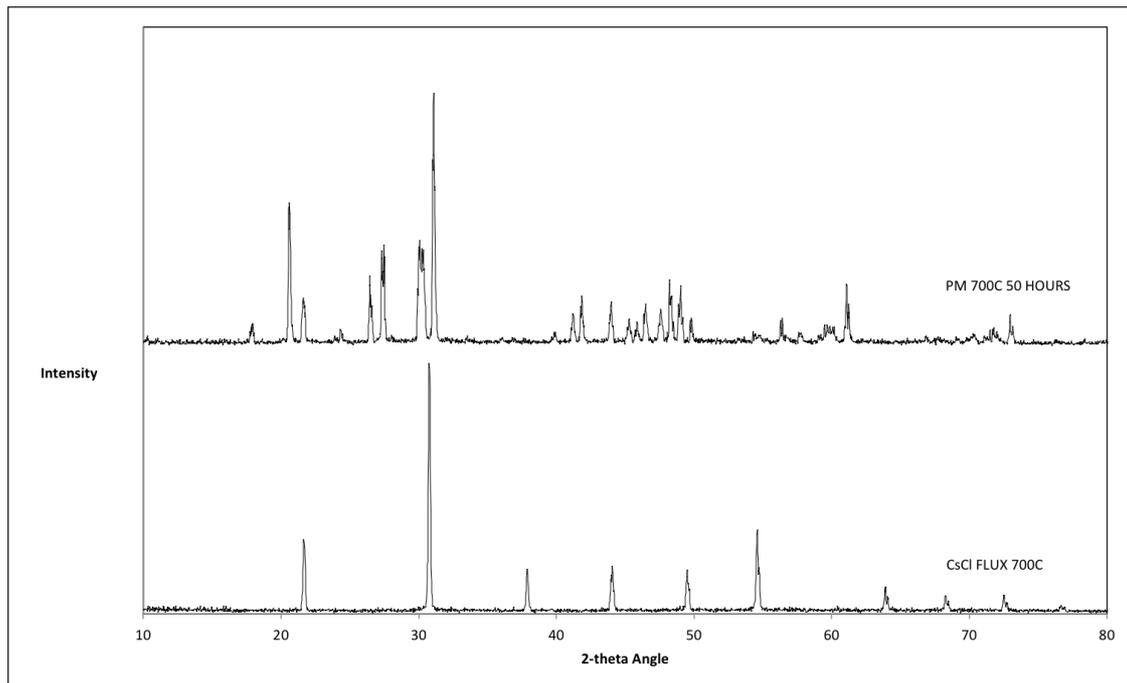
SEM images

Figure 7: Pyromorphite heated to 700°C with 1 hour isotherm
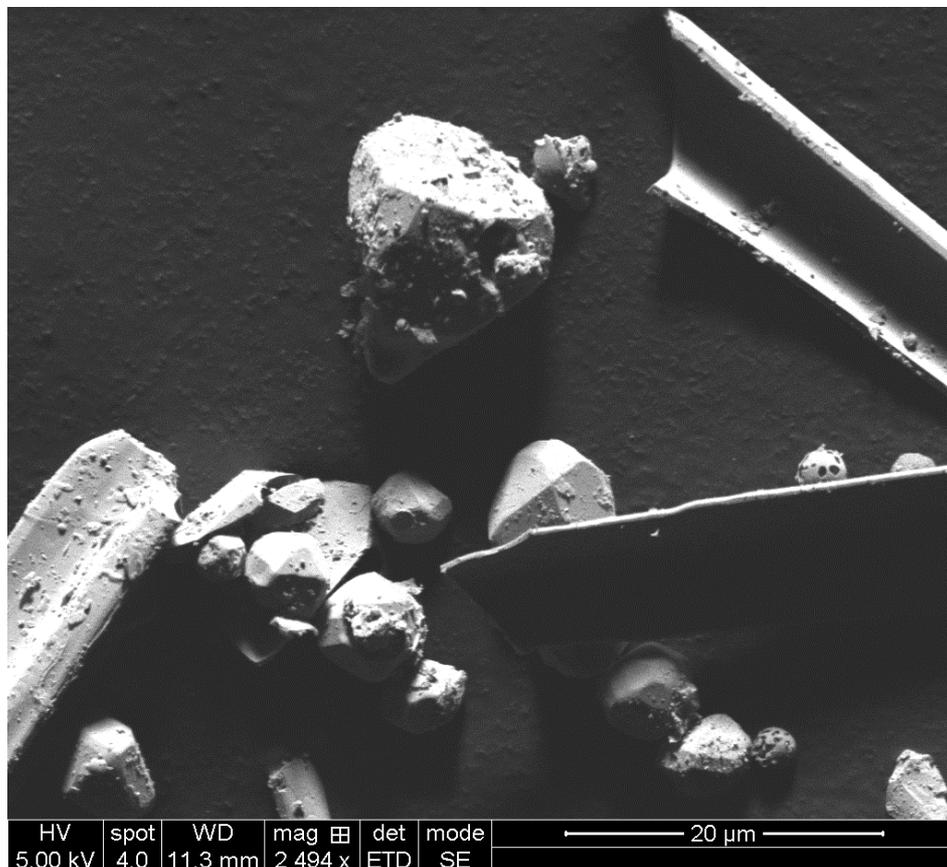
Figure 8: Pyromorphite heated to 700°C with 5 hour isotherm

HV	spot	WD	mag ⊞	det	mode	50 µm
5.00 kV	4.0	11.4 mm	951 x	ETD	SE	
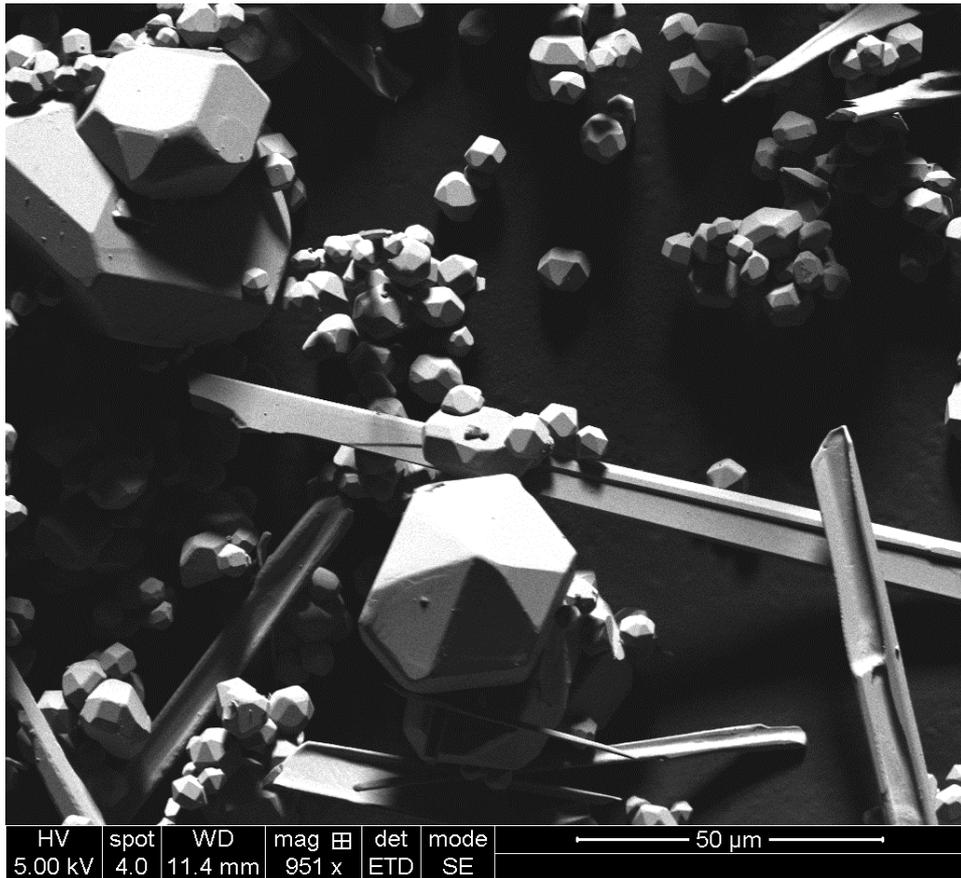
Figure 9: Pyromorphite heated to 900°C with 5 hour isotherm

HV	spot	WD	mag ⊞	det	mode	40 µm
10.00 kV	4.0	12.0 mm	1 660 x	ETD	SE	Plasma Treated
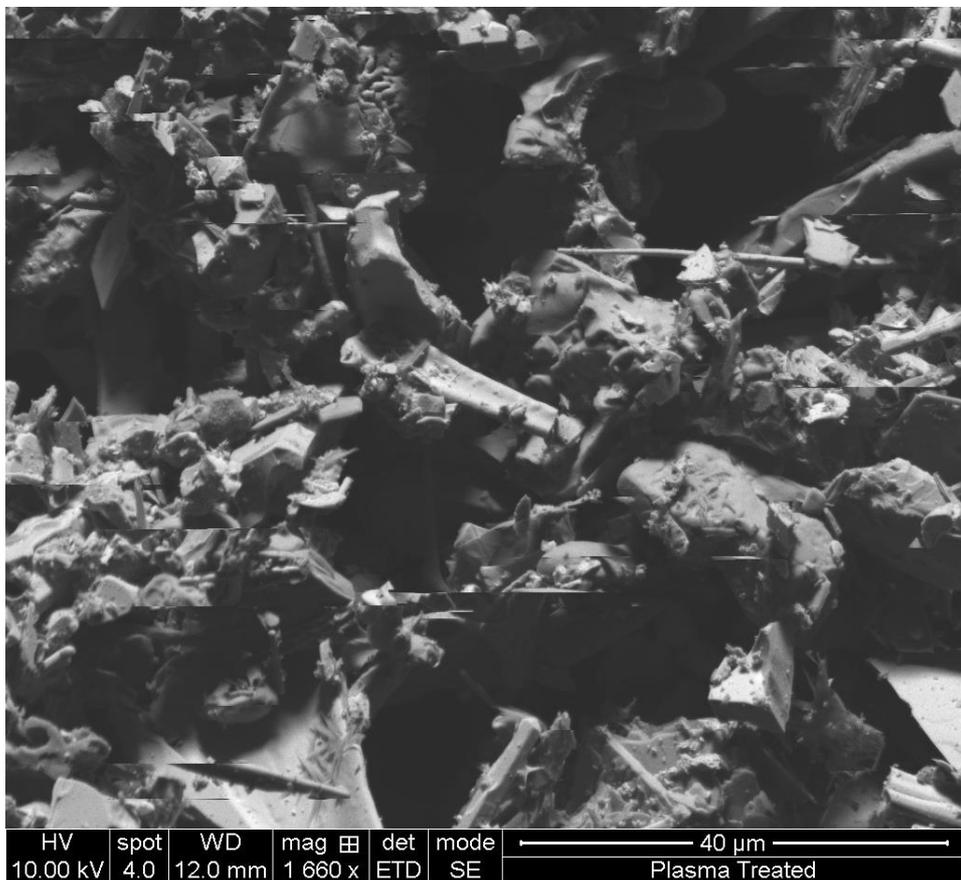
Figure 10: Pyromorphite heated to 700°C with 5 hour isotherm followed by 50-hour cooling step

HV	spot	WD	mag ⊞	det	mode	200 μm
10.00 kV	4.0	9.7 mm	299 x	ETD	SE	Plasma Treated
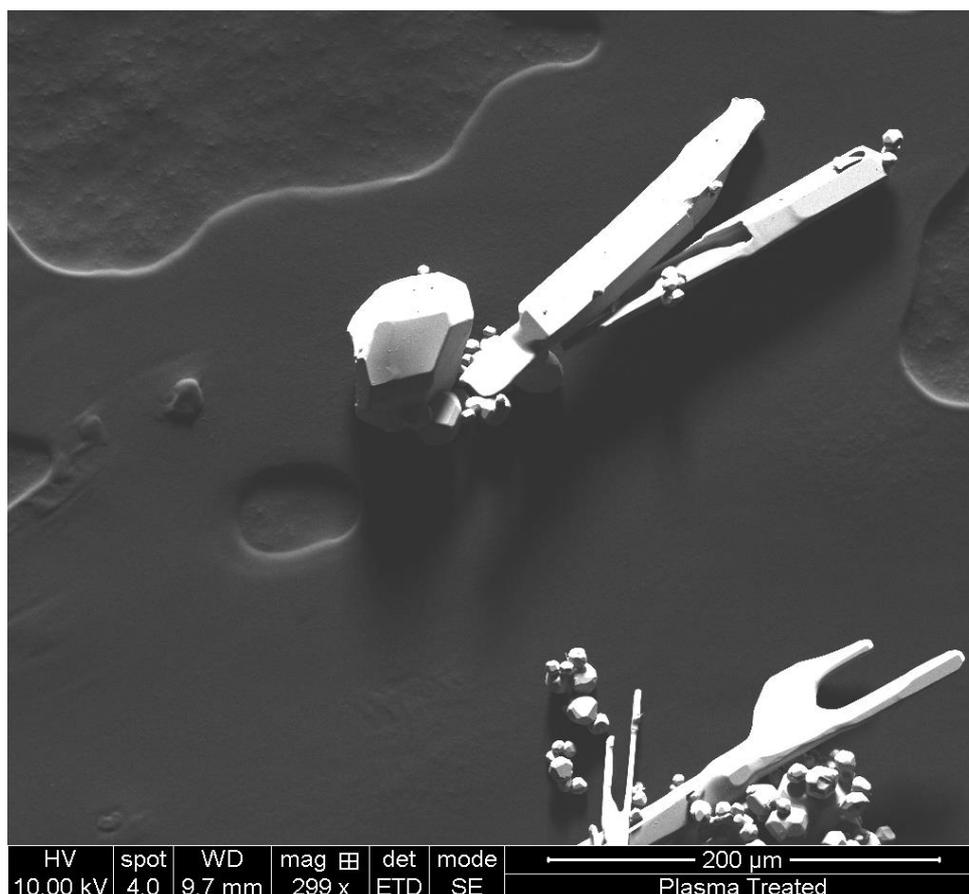
From the TGA analysis it was found that temperatures of 1000°C were too high to allow the process to be conducted on a larger scale in the nitrogen tube furnace. It was also noted that using temperatures of around 500°C was not sufficient to produce a difference in the crystallinity of pyromorphite compared to those at 1000°C. Therefore, it was decided to begin the experiments at 700°C, which is also just above the melting point of the caesium chloride (645°C).[34] This temperature ensured complete saturation of the mixture to encourage crystal growth to begin by the flux technique. The isotherm length to allow complete saturation was also trialled, resulting in samples at isotherms lasting 1 and 5 hours.

Looking at the results in Figure 4, the pattern of the peaks in the XRD spectra match those in Figure 1, confirming that the crystals were pyromorphite. The SEM images, Figures 7 and 8, confirm that crystals bigger than 250nm have been produced, with the crystals in the images exhibiting sizes of around 0.02mm and 0.05mm, respectively. It was found that a longer hold resulted in the formation of slightly larger crystals when comparing Figures 7 and 8. This also supports the XRD peak patterns formed in Figure 4, as although the spectra are very similar to each other, the peaks for the 5-hour sample are very marginally narrower, indicating a more crystalline product.

The next experiment involved using the high temperatures. Masaoka et al.[30] used 900°C to successfully grow 1mm pyromorphite and mimetite crystals. The experiment consisted of heating a sample of pyromorphite mixed with caesium chloride flux to 900°C with a 5-hour isotherm; the longer isotherm hold resulted in better crystal formation, as was found in the previous experiment.

The XRD results for this experiment in Figure 5 show peak patterns consistent with the pyromorphite shown in Figure 1. However, when closely inspected, the pattern in Figure 5 contains extra peaks at 24° 2θ, 28° 2θ and 56° 2θ. It was also observed that the sample contained burnt black soot-like powder within the mixture, which suggested that heating to 900°C was too high a temperature. This impure form of pyromorphite crystal also shows through in the SEM image in Figure 9. The image displays a very unusual form of the crystals when compared to the previous experiments, with no clean specific shapes. The difference in results compared to those of Masaoka et al.[30] could be due to the different sample pans used, which could have caused a large, uneven difference in heat supplied to the alumina crucible, generating burnt grey samples that were observed in the TGA alumina pans.

For this reason, the next experiment reverted back to the lower temperature of 700°C, but included a very slow cooling stage; this is a common approach in crystal growth. The slow rate of cooling was applied between the temperatures of 700°C to 600°C, producing a 50-hour cooling stage. The resulting XRD spectra seen in Figure 6 shows a pyromorphite peak pattern; however, the commonly found doublet peak in pyromorphites displays an unusual characteristic at 30° 2θ. Not only is the peak slightly losing its distinctive doublet, but it is also broader, taking on the appearance of that seen in previous research[35] where broader peaks formed due to an increase in pH. It could also suggest the presence of an amorphous impurity. However, in terms of crystal size, the largest crystals of pyromorphite were produced successfully using this slow cooling method, as seen in the SEM image in Figure 10. The large crystals with sizes up to 0.2mm can be seen in both the distinctive prismatic hexagonal formation and the chunky needle-like structure. This confirms that a suitable method has been devised for producing large lead phosphate minerals.

In addition to this, two forms of crystal structure were observed. One is the usual hexagonal prismatic structure, a distinctive formation of apatites, while the second structure demonstrates needle-like growth. It was noted during optical microscope viewing that the needle-like crystals formed primarily on the top upmost layer of the crucible, and the round hexagonal structures were highly concentrated at the bottom. This was true for all experiments performed at the different temperatures and time frames. The optical images can be seen in Figures 11 and 12.

Figure 11: Needle-like crystals from top layer of crucible

Figure 12: Hexagonal crystals from bottom layer of crucible
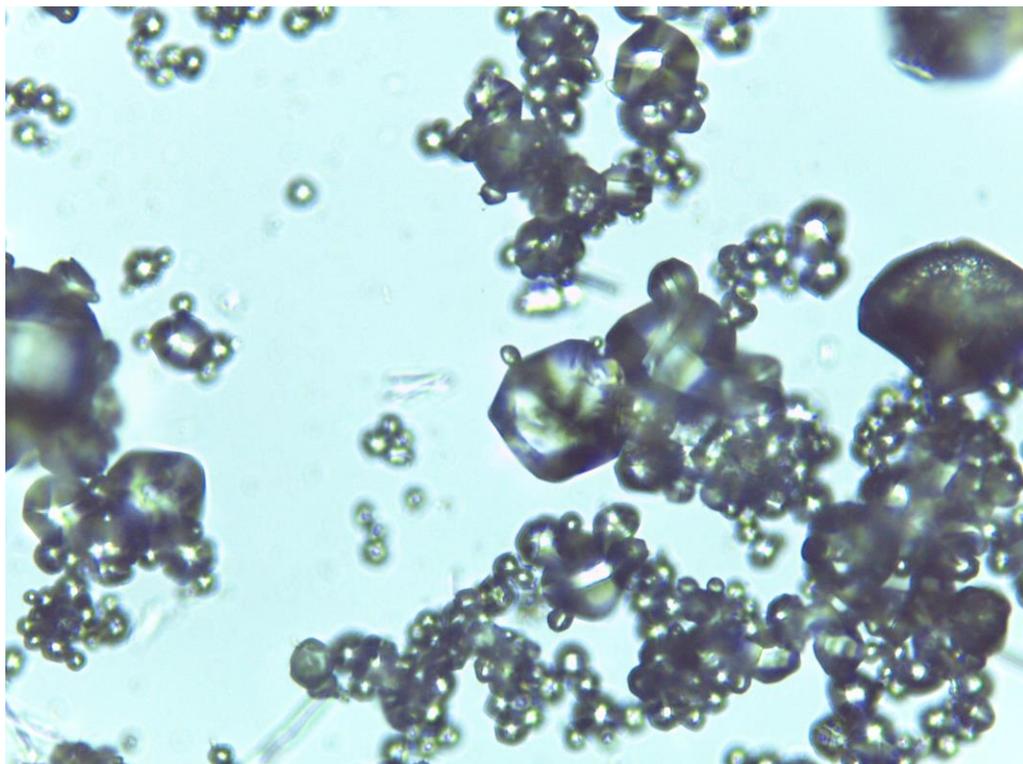
Both types of crystal were evident in all four SEM images due to the washing process, which was done for all the experiments conducted in the nitrogen furnace. In all EDXA data collected during this research, it was confirmed that no caesium elements were picked up from any of the crystal samples, confirming that the crystal washing method is sufficient in removing all traces of flux. This can also be confirmed by the XRD spectra showing no corresponding peaks to caesium chloride.

Conclusion

In this study, large pyromorphite crystals measuring up to 0.2mm in length were successfully grown using a caesium chloride flux in half the time frame of previous crystal growth studies. The research grew two types of crystal structure that were consistently exhibited, and that formed at two different positions within the crucible, suggesting a possible uneven cooling rate throughout the mixture. However, the research successfully developed a crystal washing method that was able to productively remove any traces of the caesium chloride flux without losing crystal particles, and this was confirmed using EDXA analysis.

This research has provided the opportunity to undertake further studies to probe the properties of pyromorphite using atomic force microscopy. This work can inform future efforts to ascertain how lead levels can be reduced in contaminated tap water and, thus, help to protect the environment and growing population from toxic lead.

References

1. S. Acharya, Lead between the lines, *Nature Chemistry*, 2013, **5**, 894.

2. E. G. Rowchow and E. W. Abel, *The Chemistry of Germanium, Tin and Lead: Pergamon Texts in Inorganic Chemistry*, Pergamon Press, Oxford, 1973.

3. R. E. Krebs, *The History and Use of our Earth's Chemical Elements: A reference guide,* Greenwood Press, Westport, Connecticut, 2006.

4. B. P. Lanphear, R. Hornung, J. Khoury, K. Yolton, P. Baghurst, D. C. Bellinger, R. L. Canfield, K. N. Dietrich, R. Bornschein, T. Greene, S. J. Rothenberg, H. L. Needleman, L. Schnaas, G. Wasserman, J. Graziano and R. Roberts, Low-level environmental lead exposure and children's intellectual function: an international pooled analysis. *Environmental Health Perspectives*, 2005, **113**, 894–899.

5. W. T. Wu, Y. T. Lin, S. H. Liou, C. Y. Yang, K. F. Cheng, P. J. Tsai and T. N. Wu, Brain cancer associated with environmental lead exposure: Evidence from implementation of a National Petrol-Lead Phase-Out Program (PLPOP) in Taiwan between 1979 and 2007, *Environmental International,* 2012, **40**, 97-101.

6. L. Wadanambi, B. Dubey and T. Townsend, The leaching of lead from lead-based paint in landfill environments, *Journal of Hazardous Materials,* 2008, **157**, 194-200.

7. R. Rabin, The lead industry and lead water pipes: 'A modest campaign', *American Journal of Public Health*, 2008, **9**, 1584-1592.

8. United Utilities, www.unitedutilities.com/lead-pipes.aspx, (accessed March 2016).

9. C. R. Hayes and O. D. Hydes, UK experience in the monitoring and control of lead in drinking water, *Journal of Water and Health*, 2012, **10**, 337-348.

10. S. Comber, F. Casse, B. Brown, J. Martin, P. Hillis and M. Gardner, Phosphate treatment to reduce plumbosolvency of drinking water also reduces discharges of copper into environmental surface waters, *Water and Environment Journal,* 2011, **25**, 266-270.

11. L. Barsanti and P. Gualtieric, *Algae: Anatomy, Biochemistry, and Biotechnology,* CRC Press, Florida, 2014.

12. M. Edwards, and L. S. McNeill, Effect of phosphate inhibitors on lead release from pipes, *Journal of the American Water Works Association*, 2002, **94**, 79-90.

13. J. H. Colling, P. A. E. Whincup and C. R. Hayes, The measurement of plumbosolvency propensity to guide the control of lead in tapwaters, *Journal of the Institution of Water and Environmental Management*, 1987, **1**, 263-269.

14. E. J. Kim, J. E. Herrera, D. Huggins, J. Braam and S. Kowoski, Effect of pH on the concentrations of lead and trace contaminants in drinking water: A combined batch, pipe loop and sentinel home study, *Water Research*, 2011, **45**, 2763-2774.

15. D. A. Lytle, T. J. Sorg and C. Frietch, Accumulation of arsenic in drinking water distribution systems, *Environmental Science and Technology*, 2004, **38**, 5365–5372.

16. J. R. Van Wazer, *Phosphorus and its Compounds*, Interscience Publishers, New York, 1958.

17. R. W. McDowell, A. N. Sharpley, L. M. Condron, P. M. Haygarth and P. C. Brookes, Processes controlling soil phosphorus release to runoff and implications for agricultural management, *Nutrient Cycling in Agroecosystems*, 2001, **59**, 269-284. doi:10.1023/A:1014419206761

18. D. T. Tang and R. D. Armstrong, Changes and availability of P fractions following 65 years of P application to a calcareous soil in a Mediterranean climate, *Plant and Soil*, 2008, **304**, 21-33.

19. S. R. Peter, J. D. B. Featherstone and A. Lussi, Understanding the chemistry of dental erosion, *Erosive Tooth Wear*, 2014, **25**, 163-179.

20. S. T. Ramesh, N. Rameshbabu, R. Gandhimathi, M. S. Kumar and P. V. Nidheesh, Adsorptive removal of Pb(II) from aqueous solution using nano-sized hydroxyapatite, *Applied Water Science,* 2013, **3**, 105-113.

21. U. Solecka, T. Bajda, J. Topolska and M. Manecki, Structural and vibrational behaviour of pyromorphite-vanadinite solid solution series, *Geology, Geophysics & Environment*, 2015, **41**, 135-136.

22. K. Tõnsuaadu, M. Peld and V. Bender, Thermal analysis of apatite structure, *Journal of Thermal Analysis and Calorimetry,* 2003, **72**, 363-371.

23. Y. Dai and J. M. Hughes, Crystal-structure refinements of vanadinite and pyromorphite, *Canadian Mineralogist,* 1989, **27**, 189-192.

24. J. C. Elliot, *Structure and Chemistry of the Apatites and Other Calcium Orthophosphates,* Elsevier Science, Amsterdam, 1994.

25. L. Calderin, M. J. Stott and A. Rubio, Electronic and crystallographic structure of apatites, *Physical Review B*, 2003, **67**. doi:10.1103/physRevB.67.134106

26. A. V. Shevade, L. Erickson, G. Pierzynski, and S. Jiang, Formation and stability of substituted pyromorphite: A molecular modeling study, *Journal of Hazardous Substance Research*, 2001, **3**, 2-1 to 2-12.

27. Royal Society of Chemistry, www.rsc.org/periodic-table/element/78/platinum, (accessed March 2016).

28. Royal Society of Chemistry, www.rsc.org/periodic-table/element/41/niobium, (accessed March 2016).

29. A. Akao, H. Aoki, Y. Innami, S. Minamikata and T. Yamada, Flux growth and crystal structure of pyromorphite, *Reports of the Institute for Medical and Dental Engineering,* 1989, **23**, 25-29.

30. M. Masaoka, A. Kyono, T. Hatta and M. Kimata, Single crystal growth of $Pb_5(P_xAs_{1-x}O_4)_3Cl$ solid solution with apatite type structure, *Journal of Crystal Growth,* 2006, **292**, 129-135.

31. I. Denry, J. A. Holloway and P. K. Gupta, Effect of crystallization heat treatment on the microstructure of niobium-doped fluoroapatite glass-ceramics, *Journal of Biomedical Materials Research Part B: Applied Materials,* 2012, **100B**, 1198-1205.

32. K. Tõnsuaadu, K. A. Gross, L. Plūduma, and M. Veiderma, A review on the thermal stability of calcium apatites, *Journal of Thermal Analysis and Calorimetry,* 2012, **110**, 647-659.

33. J. D. Hopwood, R. J. Davey, M. O. Jones, R. G. Pritchard, P. T. Cardrew and A. Booth, Development of chloropyromorphite coatings for lead water pipes, *Journal of Materials Chemistry*, 2002, **12**, 1717-1723.

34. Royal Society of Chemistry, www.rsc.org/learn-chemistry/wiki/substance:cesium_chloride, (accessed March 2016).

35. C. D. Newman, unpublished work.